PHOTONICS Research

Steerable merging bound states in the continuum on a quasi-flatband of photonic crystal slabs without breaking symmetry

Xin Qi,[1] Jiaju Wu,[1,5] Feng Wu,[2] Mina Ren,[1] Qian Wei,[1] Yufei Wang,[3,6] Haitao Jiang,[1] Yunhui Li,[1,4] Zhiwei Guo,[1] Yaping Yang,[1] Wanhua Zheng,[3] Yong Sun,[1,7] and Hong Chen[1]

[1]MOE Key Laboratory of Advanced Micro-structured Materials, School of Physics Sciences and Engineering, Tongji University, Shanghai 200092, China
[2]School of Optoelectronic Engineering, Guangdong Polytechnic Normal University, Guangzhou 510665, China
[3]State Key Laboratory on Integrated Optoelectronics, Institute of Semiconductors, Chinese Academy of Sciences, Beijing 100083, China
[4]Department of Electrical Engineering, Tongji University, Shanghai 201804, China
[5]e-mail: wujiaju@tongji.edu.cn
[6]e-mail: yufeiwang@semi.ac.cn
[7]e-mail: yongsun@tongji.edu.cn

Received 17 February 2023; revised 24 April 2023; accepted 6 May 2023; posted 9 May 2023 (Doc. ID 487665); published 23 June 2023

Optical resonators with high quality (Q) factors are paramount for the enhancement of light–matter interactions in engineered photonic structures, but their performance always suffers from the scattering loss caused by fabrication imperfections. Merging bound states in the continuum (BICs) provide us with a nontrivial physical mechanism to overcome this challenge, as they can significantly improve the Q factors of quasi-BICs. However, most of the reported merging BICs are found at Γ point (the center of the Brillouin zone), which intensively limits many potential applications based on angular selectivity. To date, studies on manipulating merging BICs at off-Γ point are always accompanied by the breaking of structural symmetry that inevitably increases process difficulty and structural defects to a certain extent. Here, we propose a scheme to construct merging BICs at almost an arbitrary point in momentum space without breaking symmetry. Enabled by the topological features of BICs, we merge four accidental BICs with one symmetry-protected BIC at the Γ point and merge two accidental BICs with opposite topological charges at the off-Γ point only by changing the periodic constant of a photonic crystal slab. Furthermore, the position of off-Γ merging BICs can be flexibly tuned by the periodic constant and height of the structure simultaneously. Interestingly, it is observed that the movement of BICs occurs in a quasi-flatband with ultra-narrow bandwidth. Therefore, merging BICs in a tiny band provide a mechanism to realize more robust ultrahigh-Q resonances that further improve the optical performance, which is limited by wide-angle illuminations. Finally, as an example of application, effective angle-insensitive second-harmonic generation assisted by different quasi-BICs is numerically demonstrated. Our findings demonstrate momentum-steerable merging BICs in a quasi-flatband, which may expand the application of BICs to the enhancement of frequency-sensitive light–matter interaction with angular selectivity.

https://doi.org/10.1364/PRJ.487665

1. INTRODUCTION

Trapping electromagnetic waves in optics systems is critical for enabling strong light–matter interactions that facilitate high-performance optical devices. To achieve high quality (Q) factors so that electromagnetic waves can be trapped for a longer period before decaying, a variety of resonant structures have been proposed [1–7]. Nevertheless, the Q factors of these localized states are fundamentally limited by inevitable radiative losses and defects in the fabrication process [8]. Thus, there has been a persistent desire for achieving a perfect bound state where electromagnetic waves can be localized for an infinite time.

Recently, a novel class of localized states, so-called bound states in the continuum (BICs), has greatly attracted researchers' attention [8–10]. A surprising feature of BICs is that they theoretically process infinite Q factors even lying inside continuous spectra. Empowered by their unique features to confine light, BICs have been widely observed for various waves, including quantum waves [11–13], water waves [14,15], electromagnetic waves [16–21], and acoustic waves [22–26]. To date, researches on BICs have emerged in various optical platforms

such as metamaterials [27–30] and photonic crystals (PhCs) [31–44], relying on their flexible block construction and size-dependent spectral scalability. BICs are generally divided into two categories: symmetry-protected and accidental. Symmetry-protected BICs are usually fixed at high-symmetry points in the Brillouin zone [27,28], i.e., the Γ point, where the states are completely decoupled from continuous spectra due to incompatible symmetry with outgoing waves in the radiation channels. Nevertheless, accidental BICs originate from the destructive interference between radiation channels of the system [45–48]. Therefore, accidental BICs, which usually exist at off-high symmetry points, are no longer dependent on structural symmetry but are sensitive to their spatial and geometric parameters.

In practical applications, the Q factors of BICs are intensively limited due to inevitable fabrication imperfections. An effective approach to overcome this issue is to exploit the topological properties of BICs [49–51]. BICs have been verified to be singular points of polarizations in momentum space, known as eigenmodes of an optical system whose far-field polarization direction is undefined. As a proven momentum-space vortex center for linearly polarized far fields, BICs have an integer topological charge (q). The topological nature ensures the robust existence of BICs as long as C_2^z and σ_z symmetries of the system are preserved [51]. Topological charge conservation indicates that BICs can be moved in reciprocal space with the symmetry of the system unchanged [52]. Thus, multiple isolated BICs can be tuned to the same wave vector to construct merging BICs by carefully varying structural parameters. For example, Jin *et al.* revealed that by changing the period of the structure, eight accidental BICs and one symmetry-protected BIC can be merged at the Γ point [53]. Kang *et al.* showed that by breaking the symmetries of the structure, merging BICs can be tuned in momentum space [54,55]. These works open the door to exploring merging BICs in the optical system, whose ultrahigh Q factors are robust against fabrication imperfections. Compared with merging BICs at Γ point, it is more difficult to control BICs to merge at the off-Γ point and manipulate its position in momentum space, which usually requires breaking the symmetry of the structure to achieve. However, the breaking of structural symmetry leads to complexities associated with fabrication, which constrains the universality and promotion of merging BICs. Thus, using a simple method without breaking symmetry to implement merging BICs at arbitrary points is of significant importance.

On the other hand, though Γ and off-Γ merging BICs can significantly enhance the Q factors of quasi-BICs in a wide range of wave vectors, the resonance wavelength will shift obviously with the increase of incident angle due to the dispersive band. Therefore, in practical applications, tiny dispersion is meaningful to stabilize the operating wavelength of quasi-BICs, especially for those evolved from off-Γ merging BICs. As far as we know, the current research on flatband BICs [56] provides an excellent mechanism for combining a moiré flatband with a quasi-BIC by controlling the twist angle and the distance of bilayer PhC slabs. Such single moiré BICs offer a new avenue to overcome the problem of angular sensitivity. However, the performance always suffers from scattering loss caused by fabrication imperfections. Thus, utilizing flatband merging BICs to realize angle and disturbance robustness is significant and useful.

In this paper, we propose a new scheme to construct merging BICs at almost arbitrary wave vectors on a quasi-flatband without breaking the structural symmetry. A symmetry-protected BIC can be designed at Γ point by using a PhC with C_{4v} symmetry. At off-Γ points, a few accidental BICs can be formed by adjusting the structural parameters. Since the symmetry of the structure is preserved when only the periodic constant a is changed, the symmetry-protected BIC is fixed at Γ point, while accidental BICs will move their positions in momentum space owing to their sensitivity to structural parameters. Thus, as we first increase the periodic constant a, the accidental BICs near Γ will move towards the center of the Brillouin zone (Γ) along ΓX and ΓY directions, and merge with the symmetry-protected BICs pinned at the Γ point. Since these accidental BICs have the same topological charge, they cannot annihilate each other. Owing to the restriction of the square lattice symmetry, they are also unable to further form higher-order BICs, and will therefore deflect in ΓM direction. A perfect accidental BIC does not exhibit the Fano feature at a certain oblique incidence angle since it is decoupled from far-field radiation. However, incident light will cause sharp Fano resonances when we slightly change the structural parameters, such as periodic constant a. The variation of structural parameters will affect the wave vector and amplitude of the resonance, resulting in the moving of accidental BICs. Next, we show that one accidental BIC and another accidental BIC gradually approach each other along ΓX direction by decreasing a and finally merge at off-Γ points. Since the topological charges of the two accidental BICs are opposite, they will eventually annihilate into a quasi-BIC, as governed by charge conservation. Furthermore, we demonstrate that the merging at off-Γ points can occur at any arbitrary wave vector by adjusting structural parameters without breaking symmetry. Compared with an isolated BIC, merging multiple BICs at Γ point or off-Γ points can improve the scaling property from $Q \propto k^{-2}$ to $Q \propto k^{-6}$ or $Q \propto k^{-4}$, respectively. Especially, such Γ and off-Γ merging BICs occur on an isolated band with flat dispersion, which means that they have a more stable frequency under varying oblique incidence angles. Finally, as an example of application, efficient angle-insensitive second-harmonic generation (SHG) assisted by merging BICs is demonstrated. Such steerable merging BICs on a quasi-flatband provide an excellent mechanism to design a variety of optical devices that require high Q factors, including low-threshold lasers [34,57,58], ultrasensitive sensing [59,60], nonlinear optics [29,61–63], and narrowband filters [64].

2. DESIGN AND MECHANISM

To demonstrate that merging BICs can be manipulated without reducing structural symmetry, we consider a PhC slab that consists of C_{4v} dielectric pillars (relative permittivity $\varepsilon_r = 12.11$) arranged in a square lattice [see Fig. 1(a)], where $a = 1090$ nm, $r = 265$ nm, and $h = 850$ nm. The energy bands of structures can be classified into TE-like and TM-like bands, corresponding to $E_z = 0$ and $H_z = 0$, respectively at the

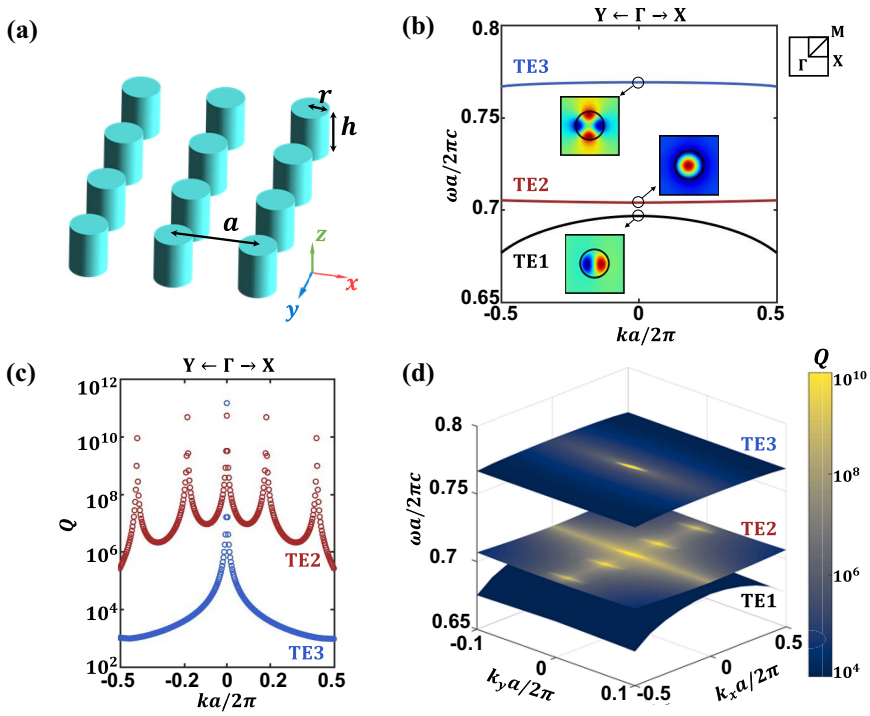

Fig. 1. (a) Schematic of the proposed PhC slab with lattice constant $a = 1090$ nm. The radius and height of the cylinder are $r = 265$ nm and $h = 850$ nm, respectively. (b) Simulated TE-like band structure. TE1, TE2, and TE3 bands are marked in black, red, and blue, respectively. The insets show the mode profiles (H_z) at Γ point on the $z = 0$ mirror plane. (c) Simulated Q factors of modes for TE2 and TE3 (red and blue circles, respectively) bands. The Q factors of the TE2 band show five divergent points along ΓX direction, which represent symmetry-protected BICs and accidental BICs. For band TE3, there is only one symmetry-protected BIC at Γ point. (d) 3D band structure including TE1, TE2, and TE3. The colors show the Q factors of the eigenmodes, and these bright spots represent BIC points. Compared with lower band TE1, band TE2 has a very narrow bandwidth, which is a quasi-flatband.

mirror plane in the z direction. The calculated TE-like bands using COMSOL Multiphysics are shown in Fig. 1(b), where we mainly focus on flatband TE2 in the middle, marked in red. The other two adjacent bands, TE1 and TE3, correspond to blue and black solid lines, respectively. The mode profiles (H_z) at Γ point for the three bands are shown in the insets of Fig. 1(b). These bands are inside the light cone where there is a continuum of radiative modes in the surrounding material. Since they are below the diffraction limit, they can radiate into free space only through zeroth-order diffraction. As shown by the red circle in Fig. 1(c), TE2 shows five BICs with infinite Q factors along high-symmetry direction ΓX, one of which is a symmetry-protected BIC fixed at Γ point and the others are accidental BICs formed by destructive interference. In contrast, for band TE3, there is only one symmetry-protected BIC at Γ point [blue circle in Fig. 1(c)]. For more clarity, we give the 3D band structure of the system as shown in Fig. 1(d). The colors represent the Q factors of the eigenmodes, which approach infinite at these BICs. As long as the symmetry of the structure is maintained, the symmetry-protected BIC will be pinned at Γ point, while the position of the accidental BIC is sensitive to structural parameters and can be moved easily in momentum space. Thus, the simultaneous existence of multiple different types of BICs on the flatband makes it possible to construct merging BICs at arbitrary wave vectors with nearly constant frequency. It should be noted that since the isolated BICs are all located in ΓX and ΓY, the formation of merging BICs will also occur in ΓX and ΓY. Therefore, the discussion on flatbands is considered along the direction of high symmetry.

A. Photonic Crystal Exhibiting a Γ Merging BIC

First, we show that four accidental BICs near the center of the Brillouin zone can be tuned to merge with the symmetry-protected BIC at Γ point. As the vortex polarization singularities (V points), the topological properties of BICs can be revealed by calculating the polarization distribution of far-field radiation, which is the projection of the Bloch wave function on a plane basis. The topological charge (q) of the polarization vortex can be defined as the winding number of the polarization vectors around a BIC in reciprocal space. That is,

$$q = \frac{1}{2\pi}\oint_C \mathrm{d}k \cdot \nabla_k \phi(k). \tag{1}$$

Here, C is a closed simple path in K space along the counterclockwise direction that surrounds the vortex center, and $\phi(k) = \arg[C_x(k) + iC_y(k)]$ is the angle of polarization where $C_x(k)$ and $C_y(k)$ denote the electric fields along x and y directions, respectively. Thus, the polarization field distribution of the vortex (antivortex) corresponds to a positive (negative) topological charge. Figure 2(a) depicts the evolution of several BICs close to the center of the Brillouin zone on band TE2 as the periodic constant a increases gradually. When

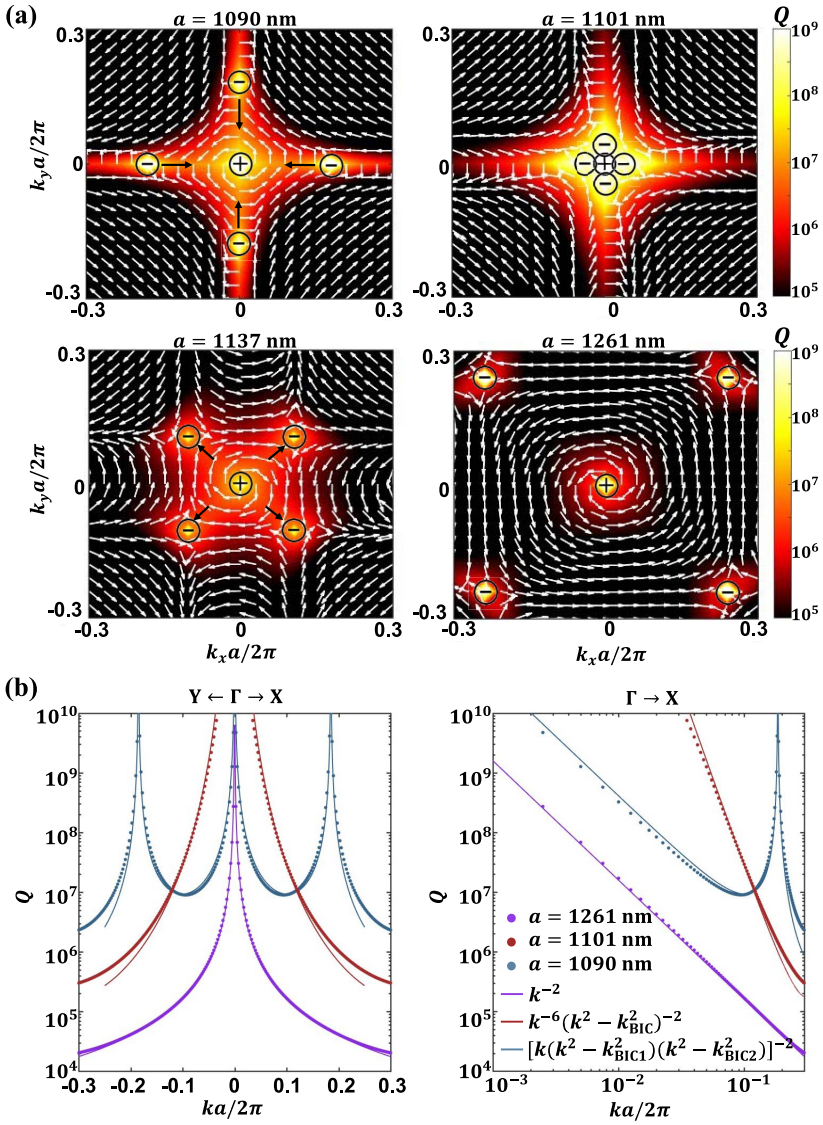

Fig. 2. (a) Simulated polarization vectors (white arrows) around the BICs near Γ point with the Q factors as the background color for the TE2 band at different periodic constants a. The black arrows indicate the moving direction of accidental BICs. When a is tuned from 1090 to 1101 nm, four accidental BICs with topological charge −1 merge with a symmetry-protected BIC with charge +1. Further increasing a, accidental BICs will deflect in the ΓM direction. (b) Simulated Q factors (dotted lines) and the corresponding fitting curves (solid lines). Q factors before ($a = 1090$ nm) and after ($a = 1261$ nm) BICs merging are marked as blue and magenta, respectively. The intermediate transient process ($a = 1101$ nm) is merging BICs, marked as red. The right panel shows the scaling rules along the ΓX direction. Compared with isolated BICs ($Q \propto k^{-2}$), the merging BICs significantly enhance the Q factors of the nearby states, which satisfy the rule $Q \propto k^{-6}$ in the vicinity of Γ.

$a = 1090$ nm, five divergent points of the Q factor can be observed, representing one symmetry-protected BIC and four accidental BICs. Polarization vortices emerge around each BIC, and topological charges of the symmetry-protected BIC and surrounding accidental BICs are $q = +1$ and $q = -1$, respectively. The symmetry-protected BIC is locked at Γ point, while the topologically protected accidental BIC will move with the change of structural parameters. As the periodic constant increases to 1101 nm, accidental BICs are close to the center along the ΓX direction and merge with symmetry-protected BICs. The merging BICs formed at Γ point significantly improve the Q factors of surrounding modes in a wide wave vector range. By further increasing a, BICs with the same topological charge of −1 cannot annihilate and will deflect in the ΓM direction as shown in the lower panel of Fig. 2(a).

To confirm the above BIC merging phenomenon, the Q factors along high-symmetry directions ΓY and ΓX at different periodic constants are provided in Fig. 2(b). The red, blue, and magenta lines represent Q factors on the TE2 band for $a = 1090$, 1101, and 1261 nm, respectively. Before charges merge at the center of the Brillouin zone ($a = 1101$ nm, red), the Q factors decay roughly as $k^{-2}(k^2 - k_{\mathrm{BIC1}}^2)^{-2}(k^2 - k_{\mathrm{BIC2}}^2)^{-2}$ away from Γ. Herein, k_{BIC1} and k_{BIC2} are wave vectors of two accidental BICs in the ΓX direction. The contribution of accidental BICs that are relatively far from Γ point to Q factors in the area discussed above cannot be ignored, so it

is taken into account when fitting curves. By increasing a, accidental BICs closest to the center gradually approach Γ and finally meet symmetry-protected BIC at $a = 1101$ nm (red). This corresponds to the merging BICs case that Q factors decay as $k^{-6}(k^2 - k_{\mathrm{BIC}}^2)^{-2}$ and are sufficiently large over a broader wave vector range around the diverging point compared with those of isolated BICs before merging. If we further increase the period to 1261 nm, the accidental BICs will be kicked away from Γ point along the ΓM direction, leaving only one symmetry-protected BIC at Γ point. In that case, the Q factor is almost not affected by accidental BICs in a small wave vector range and exhibits the rule as $Q \propto k^{-2}$ [see the magenta line in Fig. 2(b)].

So far, we have investigated the merging of BICs at the Γ point by tuning accidental BICs to merge with symmetry-protected BICs. It is relatively easy to achieve merging BICs at high-symmetry points in reciprocal space, such as Γ point. In contrast, merging multiple BICs at an off-Γ point is rare, especially if structural symmetry is preserved. In previous work, the implementation of merging BICs at an off-Γ point often needs to reduce the symmetry of the structure [54,55], which will undoubtedly bring inevitable difficulties in the fabrication process. To date, there is not yet a feasible mechanism for implementing tunable merging BICs at Γ and off-Γ points while maintaining structural symmetry. In the following, we demonstrate that merging BICs at an off-Γ point can be realized by merging two accidental BICs without breaking structural symmetry.

B. Merging BICs at Off-Γ Point

We still consider the PhC slab and focus on the Brillouin zone that deviates from Γ. As shown in Fig. 3(a), in addition to the above-mentioned accidental BIC that participates in the merging BICs of Γ point, there is another accidental BIC farther from Γ located at ΓX on the TE2 band. The far-field polarization of these two accidental BICs exhibits characteristics of the vortex (charge +1) and antivortex (charge −1), so they have opposite topological charges. By keeping other parameters unchanged and only gradually decreasing the periodic constant a, these two accidental BICs are tuned to approach each other along ΓX direction. When a decreases to 1083 nm, they meet at an off-Γ point and form merging BICs. Owing to their opposite topological charges, the two accidental BICs will annihilate each other if we further decrease a, and will evolve into a quasi-BIC as shown by the dashed circle in the last panel of Fig. 3(a), where the Q factors are not infinite but remain large and can be regarded as a supercavity. If the structure possesses higher symmetry, it is possible to merge the basic BICs into a higher-order BIC at an off-Γ point. In the above evolutionary process, the symmetry-protected BIC has been fixed at the Γ point since the structural symmetry has not been changed. We also give the Q factors distribution in the ΓX direction as shown in Fig. 3(b), indicating that the Q factors near merging BICs (red) have been significantly enhanced over a broad wave vector compared with either isolated symmetry-protected BICs or isolated accidental BICs (blue). The Q factors decay as $k^{-2}(k^2 - k_{\mathrm{BIC1}}^2)^{-2}(k^2 - k_{\mathrm{BIC2}}^2)^{-2}$ at $a = 1090$ nm, while the Q factors of merging BICs constructed from two accidental BICs at $a = 1083$ nm follow the scaling rule as

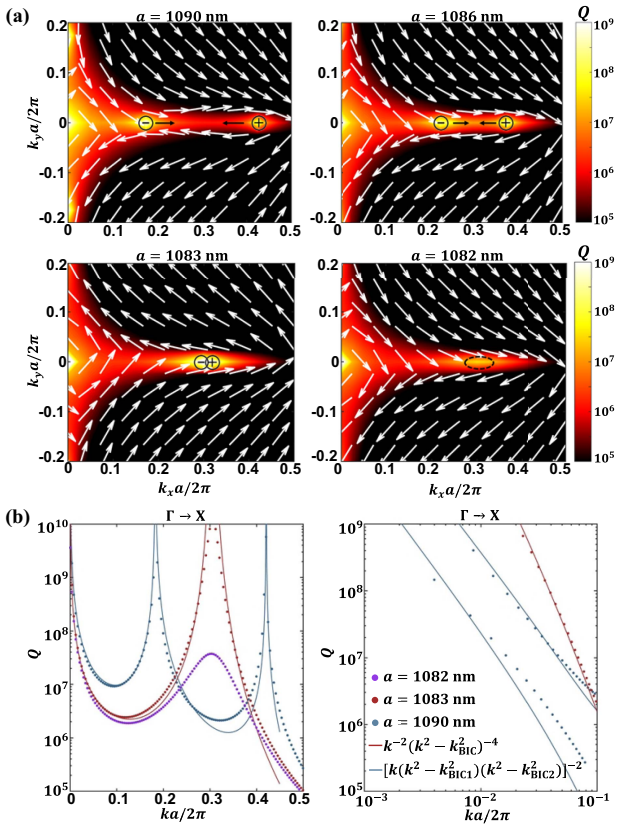

Fig. 3. (a) Simulated polarization vectors (white arrow) around the accidental BICs with Q factors as the background color for the TE2 band at different periods a. The black arrows indicate the moving direction of accidental BICs. When a is tuned from 1090 to 1083 nm, the two accidental BICs with opposite topological charges approach each other and form merging BICs at an off-Γ point. Further decreasing a, the two BICs annihilate and evolve into a quasi-BIC. (b) Simulated Q factors (dotted lines) and fitting curves (solid lines). The Q factors before ($a = 1090$ nm) and after ($a = 1082$ nm) BICs merging are marked as blue and magenta, respectively. The intermediate transient process ($a = 1083$ nm) is merging BICs, marked as red. The merging BICs case has considerably enhanced Q factors for nearby states compared with the isolated BICs case, as the dependence of Q factor on wave vectors near BICs changes from k^{-2} to k^{-4}. Even if the two BICs collide and annihilate each other, the converted quasi-BIC still maintains a high Q factor.

$Q \propto k^{-2}(k^2 - k_{\mathrm{BIC}}^2)^{-4}$, which greatly improves the performance of potential applications requiring momentum selection. The Q factors are dominated by the intrinsic loss of materials at merging BICs, and thus high-refractive-index dielectric material with ultralow intrinsic loss is an excellent choice to create a high-Q cavity (see Appendix C). It should be noted that accidental BICs originate from destructive interference between radiation channels, which is common in various optical systems. Therefore, this mechanism of using multiple accidental BICs to realize the merging phenomenon is also applicable to other systems, such as typical air-hole PhCs.

C. Merging BICs at an Arbitrary Location

Next, we demonstrate that merging BICs can be achieved at an arbitrary point in reciprocal space by changing periodic

constant a and height h simultaneously but keeping C_4^z symmetry. Whether decreasing (increasing) the periodic constant a or increasing (decreasing) the height h, the above two accidental BICs located at off-Γ point will approach (away from) each other along ΓX direction. For the change of periodic constant a, the moving speed of the two accidental BICs in momentum space is almost the same. However, the accidental BIC with topological charge −1 is much more sensitive to the height h than the one with topological charge +1, which means that by changing the height h, the different accidental BICs have different moving scales Δk_{BIC} (see Appendix A). This phenomenon of asymmetric shift may be explained by Fabry–Perot (FP) mode with different orders participating in the formation of different accidental BICs, which generally exists in the PhC slab depending on the height h. Owing to the ultralow Q factor of FP resonance, they are often regarded as the background spectrum, while the resonance properties are ignored [40]. Because the types and number of BICs have not changed during the formation of merging BICs, the phases (n_1, n_2, n_3) of BICs defined in Ref. [40] always belong to areas of (2, 1, 0), where n_1, n_2, and n_3 denote the number of accidental BICs, symmetry-protected BICs, and Friedrich–Wintgen BICs (FW-BICs), respectively. It is worth noting that this is different from previous work [55] based on FW-BIC with (1, 0, 1) phase. When the height changes, the frequency shift of lower-order FP mode is slower, so that the accidental BICs resulting from the coupling of the magnetic dipole (MD) mode and different orders of FP mode have asymmetric moving speeds. Thus, merging BICs can be designed to appear at an arbitrary point in ΓX direction as long as we choose an appropriate periodic constant a and height h simultaneously. For example, as shown in Fig. 4(a), when (a, h) is equal to (1048.7 nm, 845 nm), (1083.2 nm, 850 nm), and (1115 nm, 857 nm), we tune merging BICs to $0.4\pi/a$, $0.6\pi/a$, and $0.8\pi/a$, respectively. The Q factors satisfy the scaling rule $Q \propto k^{-2}(k^2 - k_{\mathrm{BIC}}^2)^{-4}$ shown in Fig. 4(b), which further confirms the existence of merging BICs.

D. Quasi-Flatband

Above, we have proved that merging BICs can be constructed at arbitrary wave vectors while maintaining structural symmetry. The unique topological property of BICs ensures that Q factors can be greatly improved in a larger wave vector range by merging several BICs that are robust against fabrication imperfections (see Appendix B) and improve the performance of optoelectronic devices. However, merging BICs at either Γ point or off-Γ point usually occur in a band with large dispersion [54,55,65], which limits its performance in many practical applications based on angle selectivity and stable operating frequency. Next, by comparing the resonance modes near Γ point on TE1 and TE3 energy bands, we prove that the quasi-BIC evolved from a merging BIC on flatband TE2 is insensitive to the incident angle, not only in terms of Q factors but also the resonance wavelength. At $a = 1101$ nm, a merging BIC is formed at Γ point on the TE2 band [red line in Fig. 2(b)], while there is always an isolated symmetry-protected BIC on the TE3 band [blue circle in Fig. 2(b)] due to the maintenance of structural symmetry. We consider that the PhC slab is illuminated by a TE obliquely incident plane wave polarized along the y axis. As the incident angle increases from 0°, the two BICs transform into quasi-BICs. We call the quasi-BIC that evolves from symmetry-protected BIC as quasi-BIC1, and that from merging BICs as quasi-BIC2. The simulated transmittance spectra of two quasi-BICs under different

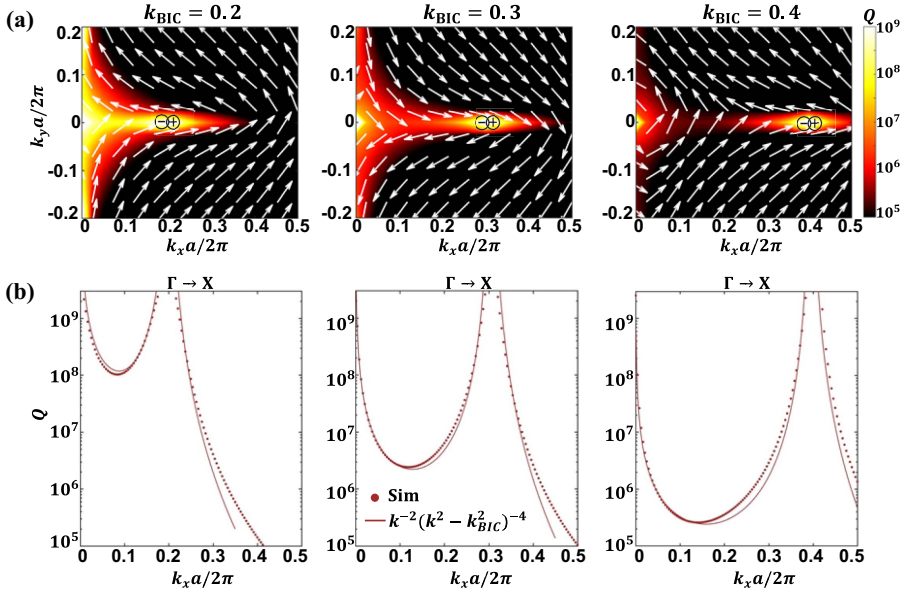

Fig. 4. (a) Simulated polarization vectors (white arrows) around accidental BICs at different wave vectors with Q factors as the background color for the TE2 band. The wave vectors of merging BICs at $0.4\pi/a$, $0.6\pi/a$, and $0.8\pi/a$ correspond to a, h of (1048.7 nm, 845 nm), (1083.2 nm, 850 nm), and (1115 nm, 857 nm), respectively. By properly selecting parameters a and h, merging BICs can be realized at almost any wave vector position. (b) Simulated Q factors (dotted lines) and fitting curves (solid lines) corresponding to merging BICs at different wave vectors. The merging BICs located at arbitrary wave vectors follow the scaling rule as $Q \propto k^{-2}(k^2 - k_{\mathrm{BIC}}^2)^{-4}$.

incident angles are shown in Figs. 5(a) and 5(b). At normal incidence ($\theta = 0°$), one symmetry-protected BIC and one merging BIC exist in TE3 and TE2, respectively, having vanishing linewidths, and the electric dipole (ED) resonance mode located on TE1 can be observed. The isolated BIC on the TE3 band can be tailored, and the dispersion can be flattened to reduce the sensitivity to the angle of incidence; see Figs. 1(b) and 5(a). Nevertheless, the Q factor of the flattened quasi-BIC1 drops rapidly as the incident angle increases, as shown in Fig. 5(a). Interestingly, by precise design, we can achieve merging BICs in a flattened band that possesses an ultrahigh Q resonance with a certain degree of incident-angle robustness. One can see from Fig. 5(b) that the resonance wavelength and the Q factors of quasi-BIC2 are nearly unchanged even at a large incident angle. As θ increases from 0° to 12°, the relative shift of ED mode $\Delta\lambda/\lambda_0$ is equal to 1%, where $\Delta\lambda$ is the resonance peak wavelength shift, and λ_0 is the wavelength when $\theta = 0°$, while that of quasi-BIC2 is only 0.1%.

To gain deep insight into the spectral response of the two distinct quasi-BICs and the ED mode, we first calculated the scattering powers of different multipoles of three resonance modes in the Cartesian coordinate system based on multipole scattering theory [66], as visualized in Figs. 5(d)–5(f). It can be observed from Fig. 5(e) that the contribution of the electric quadrupole (EQ) moment (orange line) is dominant, which indicates that the strong Fano resonance (quasi-BIC1) is mainly induced by the EQ moment. Different from quasi-BIC1, quasi-BIC2 stems from MD resonance since the contribution of the MD moment (red line) is dominated, as shown in Fig. 5(f). To further understand that the merging BIC occurs in the flatband, we choose quasi-BIC2 at 1551 nm as the operating wavelength and give the magnetic field distribution of the structure under different incident angles, as shown in Fig. 5(c). One can see that the magnetic fields can be strongly enhanced as the incident angle changes because the Q factors and resonance wavelength of quasi-BIC2 are almost unchanged as the incident angle increases. Namely, quasi-BIC2 is located in a flatband. For comparison, we also choose a conventional ED mode at 1567 nm as the operating wavelength and also give the magnetic field distribution of the structure under different incident angles, as shown in Fig. 5(d). It can be seen that, compared with the flat BIC2, the enhancement of magnetic fields assisted by conventional ED mode at 1567 nm is rapidly changed under different incident angles. Since the formation of resonance-trapped BICs in metamaterial originates from local resonance in structural elements that can be excited by plane waves in different directions, they are insensitive to the incident angle and therefore correspond to almost flat bands [67,68]. Note that merging BICs within a flatband would be very useful in some applications as shown below.

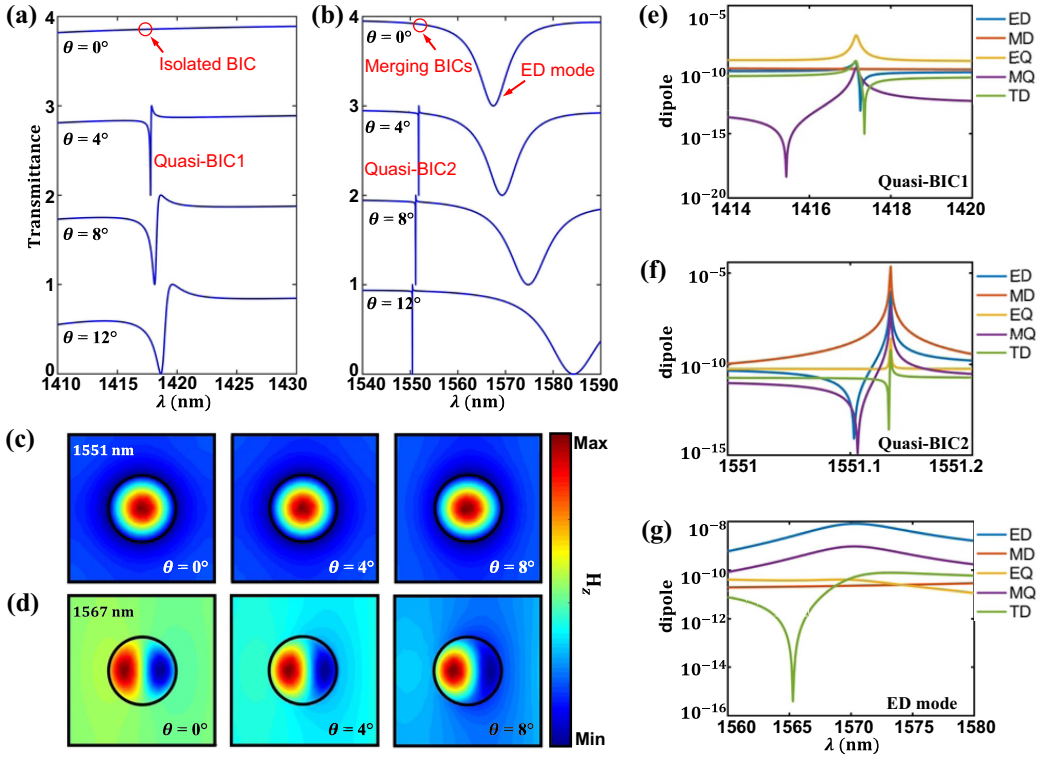

Fig. 5. (a) Transmission spectra of the quasi-BIC1 originated from isolated BIC at TE3 under different incident angles θ. (b) Transmission spectra of quasi-BIC2 originated from isolated BIC at TE2 and ED mode at TE2. The structural parameters satisfy the condition of the above-mentioned merging BICs at Γ point, i.e., (a, h) are (1101 nm, 850 nm). With the increase of θ, the linewidth of quasi-BIC1 increases obviously, while quasi-BIC2 always keeps an extremely narrow linewidth. Owing to the existence of a quasi-flatband, the wavelength of quasi-BIC2 is almost unchanged. (c), (d) Magnetic field distributions with different incident angles at 1551 nm (top) and 1567 nm (bottom), respectively. Compared with ED mode, even at a large incident angle, the highly localized MD mode of the electromagnetic field is still stable at the wavelength of merging BIC. (e)–(g) Contributions of different multipolar excitations for (e) quasi-BIC1, (f) quasi-BIC2, and (g) ED mode of the PhC slab at $\theta = 4°$.

E. Efficient SHG Enhanced by Flat Merging BICs

Finally, we investigated the superior performance in the enhancement of SHG by flatband merging BICs. AlGaAs is chosen as the material of a dielectric cylinder, which has been widely used for SHG owing to its large second-order nonlinear coefficient $\chi^{(2)}$ and excellent broadband transparency. For the dispersion of the refractive index of AlGaAs, we used the analytical model proposed in Ref. [69]. We first consider merging BICs at Γ point. At $a = 1101$ nm, $r = 265$ nm, and $h = 850$ nm, the numerically simulated transmission spectra of quasi-BIC1 and quasi-BIC2 by sweeping incident angle θ are given in Figs. 6(a) and 6(b), respectively. It is clear that quasi-BIC1 is almost obscured by the surrounding background when θ reaches 15°, while quasi-BIC2 still maintains an extremely narrow linewidth, and its relative shift is only approximately 0.12%, which exhibits an excellent ability to enhance SHG. The SHG efficiency is defined as

$$\eta = \frac{\iint_A^0 \boldsymbol{S}_{\mathrm{SH}} \cdot \hat{\boldsymbol{n}} \mathrm{d}a}{I_0}, \tag{2}$$

where $\boldsymbol{S}_{\mathrm{SH}}$ represents the Poynting vector of the SH field, $\hat{\boldsymbol{n}}$ is the unit vector normal to a surface A enclosing the cylinder, and I_0 is the pump intensity ($I_0 = 1$ kW/cm^2 and $\chi^{(2)} = 100$ pm/V [70] in the simulations). For comparison, we first calculate the efficiency of SHG enhanced by quasi-BIC1 at $\theta = 2°, 4°$, and 8° as shown in Fig. 6(c). Since the Q factor of an isolated BIC is sensitive to the incident angle, it can be seen that the efficiency of SHG decreases sharply with the slight increase of θ. Then, the efficiency of SHG enhanced by the above designed quasi-BIC2 with a flatband is calculated in Fig. 6(d). The three panels represent incident angles of 4°, 8°, and 12°, respectively. We can see that even if the larger incident angle is changed, the efficiency is still not reduced, and the relative shift of the resonant wavelength is tiny. At $\theta = 4°$, the nonlinear signal at the flatband wavelength is further enlarged, which is nearly two orders of magnitude higher than that at quasi-BIC1.

Generally, using a quasi-BIC to enhance SHG is based on symmetry-protected BICs [29,30,71–73]. This means that the conversion efficiency can be significantly improved only at a small incident angle, as for the quasi-BIC1 mentioned above. BICs merged at off-Γ provide an excellent way to overcome the limitation of incident angle. When (a, h) are (1083.2 nm, 850 nm), the linewidth of the transmission spectrum vanishes

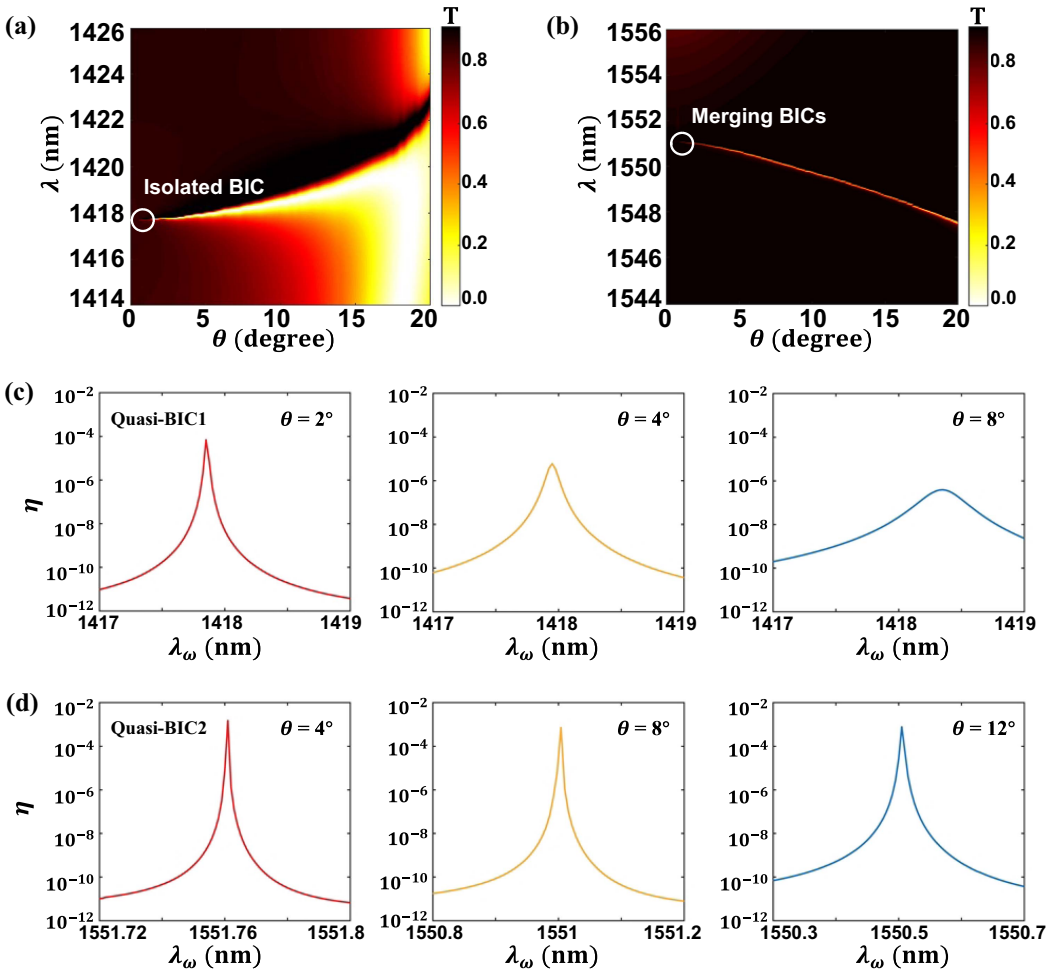

Fig. 6. (a), (b) Simulated transmission spectra of different quasi-BICs by sweeping θ from 0° to 20°. (c), (d) Efficiency of SHG enhanced by (c) quasi-BIC1 and (d) quasi-BIC2 at different incident angles θ. Compared with the quasi-BIC1, quasi-BIC2 has advantages in both efficiency and wavelength stability, especially for increased θ.

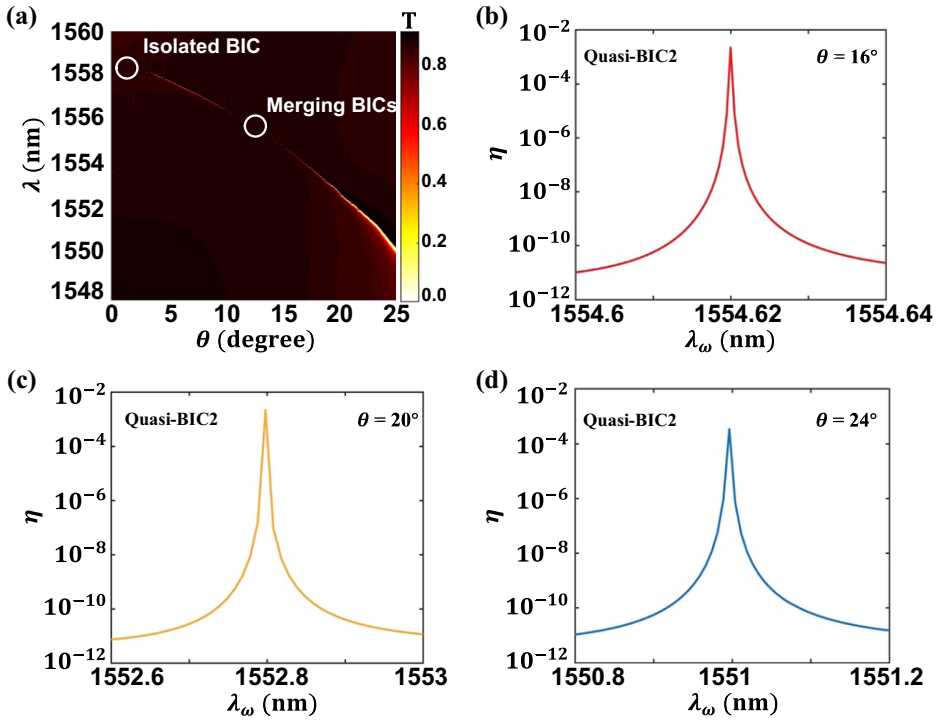

Fig. 7. (a) Simulated transmission spectra of merging BICs at off-Γ point by sweeping from 0° to 25°. (b)–(d) Efficiency of SHG enhanced by quasi-BIC2 at $\theta = 16°$, 20°, and 24°, respectively. Owing to the existence of merging BICs at off-Γ, high-efficiency SHG can still be achieved at a huge oblique incidence angle.

at a certain incident angle as shown in Fig. 7(a). The simulated SHG with different incident angles θ in Figs. 7(b)–7(d) clearly shows the unique advantages of merging BICs at off-Γ; even at a large oblique incidence angle, it can still maintain an efficient and stable SHG in a certain angle range. It is worth mentioning that no matter whether SHG is enhanced by merging BICs at Γ point or off-Γ point, the wavelength with maximum values of η basically does not shift. As the angle increases by 8°, the relative shifts are all less than 0.3%. Hence, we can deduce that quasi-BICs originated from flatband merging BICs exhibit highly efficient performances in various applications requiring field enhancement.

3. CONCLUSIONS

In summary, without breaking structural symmetry, we have proposed a feasible avenue to construct merging BICs at almost arbitrary points in momentum space. The proposed structure satisfies C_4^z symmetry and supports the concurrence of symmetry-protected BICs and a few accidental BICs. The topological property of BICs ensures that accidental BICs can be moved in reciprocal space. By increasing the period of the PhC, the BIC near the Γ point will converge to the center of the Brillouin zone, and finally merge with the symmetry-protected BIC at Γ point. If the period decreases, these two accidental BICs carrying opposite topological charges approach each other and then form a merging BIC at off-Γ point. We further showed that merging BICs can be constructed at almost arbitrary wave vectors by selecting appropriate heights and periods. Moreover, the band on which BICs are manipulated to realize merging BICs possesses quasi-flat dispersion. Thus, these flatband merging BICs eliminate the performance limitation of quasi-BICs caused by dispersive effects under wide-angle illuminations. Finally, compared with an isolated symmetry-protected BIC, the efficiency and robustness of SHG assisted by the designed flatband merging BICs can be greatly enhanced. When merging BICs appear at off-Γ point, stable and efficient SHG at a larger incident angle is also proved. Our finding may have many potential applications based on local field enhancement, such as nonlinear, sensing, and quantum effects.

APPENDIX A: EVOLUTION OF BICS WITH THE VARIATION OF STRUCTURAL PARAMETERS

The evolution of merging BICs at Γ with the variation of the periodic constant a and height h is shown in Fig. 8. The height h is fixed at 850 nm and the periodic constant a is fixed at 1090 nm in Figs. 8(a) and 8(b), respectively. When we continuously change the parameters, the trajectory of BICs is visible in momentum space. It can be seen that a symmetry-protected BIC is pinned at Γ point, while accidental BICs are gradually moved to Γ point along ΓX direction with the increase of period or decrease of height. They finally merge and form a huge bright area on the distribution map of Q factors. After that, the accidental BICs turn away from the symmetry-protected BIC along the ΓX direction.

We also study the evolution of merging BICs at off-Γ point. With the decreasing period or the increasing height, two accidental BICs approach each other as indicated in Figs. 9(a) and 9(b), respectively. Since the topological charges of two BICs are

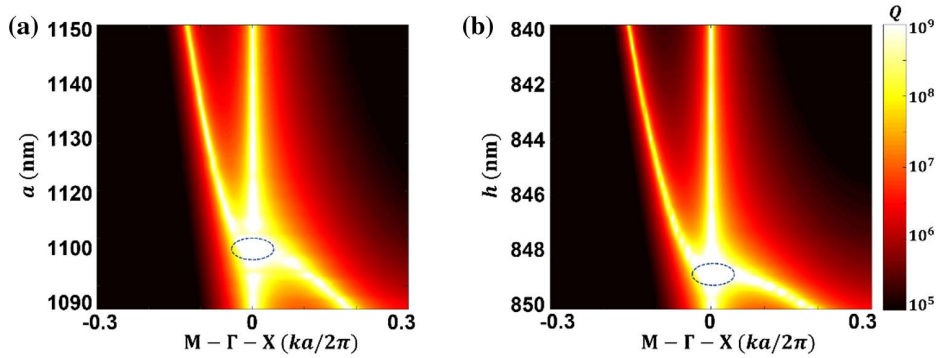

Fig. 8. Evolution of merging BICs at Γ point with different structural parameters. (a) Periodic constant a. (b) Height of cylinder h. The dotted circle represents the position of merging BICs. Other parameters are $h = 850$ nm in (a) and $a = 1090$ nm in (b).

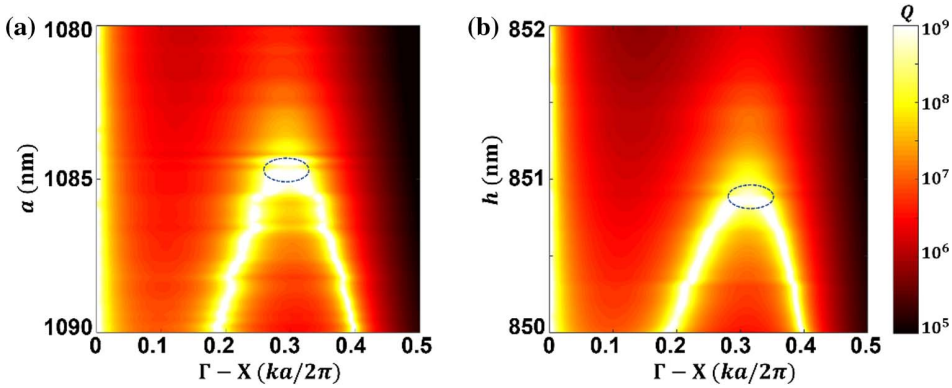

Fig. 9. Evolution of merging BICs at off-Γ point with different structural parameters. (a) Periodic constant a. (b) Height of cylinder h. The dotted circle represents the position of merging BICs. Other parameters are $h = 850$ nm in (a) and $a = 1090$ nm in (b). The position of merging BICs can be steered by adjusting parameters a and h.

opposite, if the parameters are further changed, they will be annihilated and transformed into quasi-BICs with a finite Q factor. It is worth noting that the position of a merging BIC formed by adjusting different parameters is different as indicated by the dotted circles in Figs. 9(a) and 9(b). That means that the sensitivities of accidental BICs movement to parameters a and h are different. Thus, we can adjust these two parameters simultaneously to realize merging BICs at any wave vector position as shown in Fig. 4.

APPENDIX B: ROBUSTNESS OF MERGING BICS AGAINST FABRICATION IMPERFECTIONS

The influence of three typical types of fabrication imperfections is considered in the Q factor. In the first type, the diameter of the cylinder has a deviation from the design value, as shown in Fig. 10(a). In this case, there is no broken symmetry. In the second type, the cylinder becomes a cone with different diameters on the top and bottom, as shown in Fig. 10(b). Owing to the disappearance of up-down mirror symmetry, upward and downward radiation loss cannot be eliminated simultaneously. In the third type, the cylinder has a tilt angle, as shown in Fig. 10(c). Both in-plane symmetry and out-of-plane symmetry have been broken and BICs transformed into quasi-BICs with finite Q factors. We first consider merging BICs at Γ point. The influences of these three types of fabrication defects are shown in Figs. 10(d)–10(f). Compared with isolated symmetry-protected BICs on TE3, Q factors of merging BICs located at TE2 remain sufficiently large in a broad wave vector under different degrees of defects.

Next, we consider the merging BICs at off-Γ point. Compared with the isolated accidental BIC, merging BICs at off-Γ point are similarly superior in a broad wave vector range, as shown in Fig. 11. It is worth noting that merging BICs at Γ point are more robust to structural defects than those at off-Γ point. On one hand, this is because a symmetry-protected BIC is protected by in-plane symmetry C_{4v} and does not disappear by broken up-down mirror symmetry. On the other hand, the accidental BICs that participate in the formation of the merging BIC at Γ point have the same topological charge, which means that they will not be annihilated due to defects, and the BIC that provides a high Q factor for the proximate mode always exists.

APPENDIX C: INTRINSIC LOSS OF MATERIALS

The loss of the system is mainly composed of intrinsic loss caused by materials and radiation loss, following

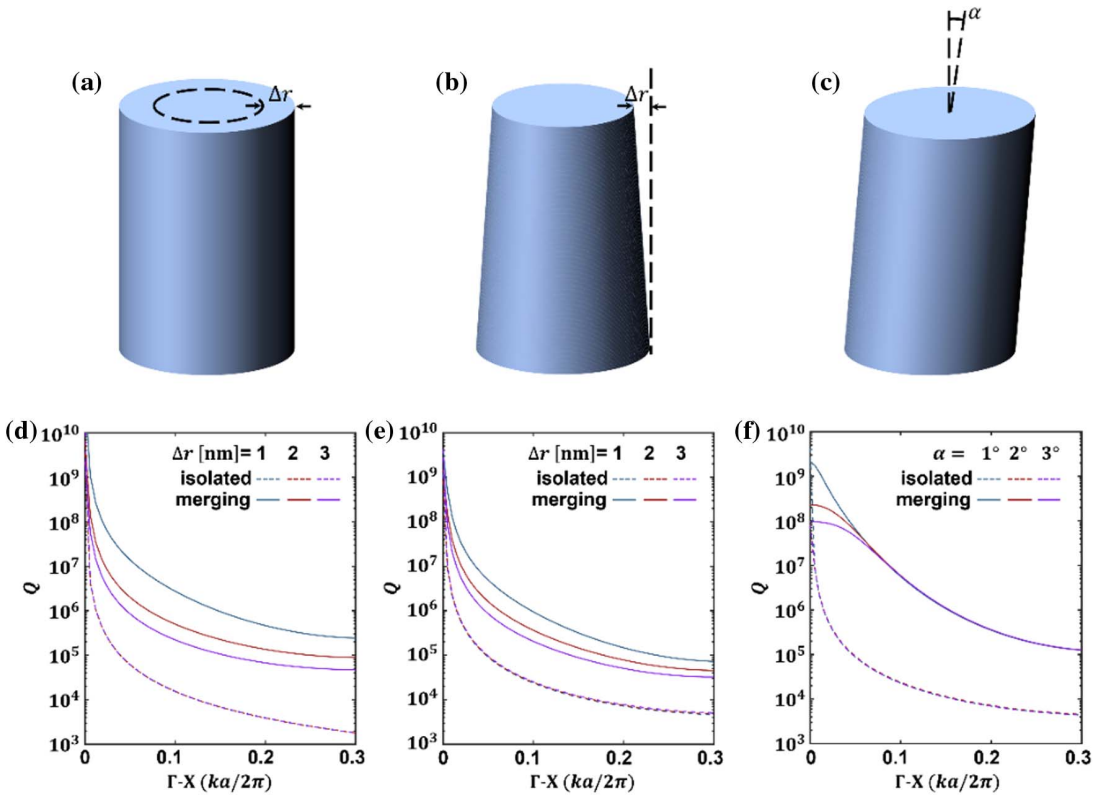

Fig. 10. Influence of fabrication defect on Q factor for BICs at Γ. Cylinder in the unit cell with (a) deviated radius, (b) different radii on the top and bottom, and (c) tilted angle. (d)–(f) Q factor evolution near merging BICs (solid lines) and isolated BIC (dashed lines) at Γ point under parameter variations shown in (a)–(c), respectively. Here, apart from the varying parameters, other parameters are the same as in Fig. 2(a), i.e., $a = 1101$ nm for merging BICs.

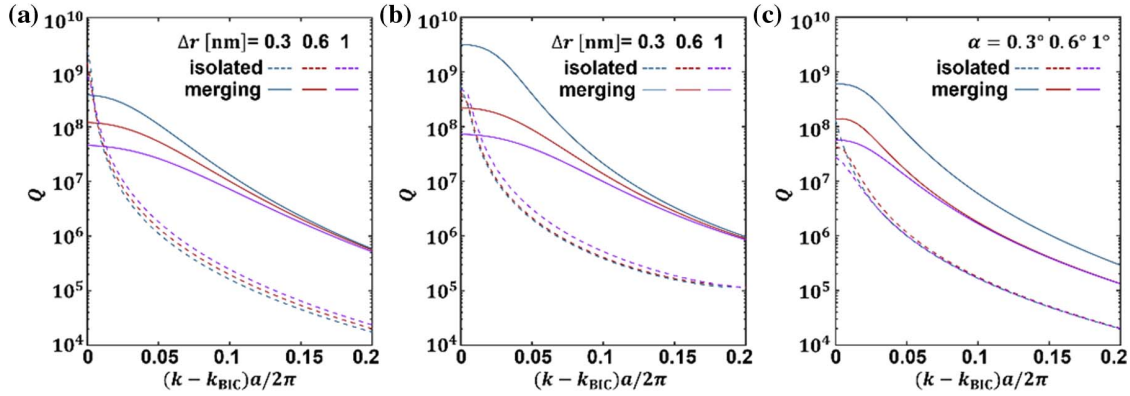

Fig. 11. Influence of fabrication defect on Q factor for BICs at off-Γ. (a)–(c) Q factor evolution near merging BICs (solid lines) and isolated BIC (dashed lines) at off-Γ point under parameter variations resulting from the above three defects, respectively. Here, apart from the varying parameters, other parameters are the same as in Fig. 3, i.e., $a = 1083$ nm for the merging BICs and $a = 1090$ nm for the isolated BIC.

$\gamma_{\mathrm{Total}} = \gamma_{\mathrm{in}} + \gamma_{\mathrm{rad}}$. For merging BICs, the radiation loss is eliminated due to the destructive interference between radiation channels, which means that Q factors are dominated by the intrinsic loss of materials, as shown in Fig. 12(a). Thus, dielectric materials with ultralow intrinsic loss, such as Si and TiO_2, are ideal choices to form a high-Q cavity in the wavelength range we are interested in. In our designed merging BICs at Γ and off-Γ points, the Q factors are still sufficiently large in a broad wave vector range with an unavoidable intrinsic loss [$\mathrm{Im}(n) = 10^{-6}$], as shown in Figs. 12(b) and 12(c).

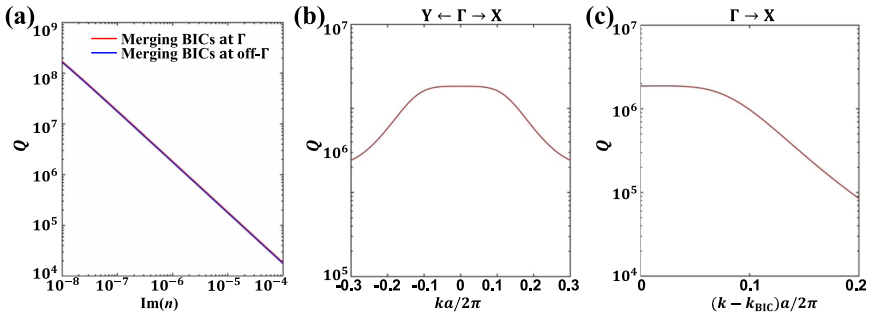

Fig. 12. Influence of intrinsic loss on merging BICs. (a) Simulation for the evolution of Q factors with different intrinsic losses of materials at merging BICs. The Q factors with intrinsic loss $\mathrm{Im}(n) = 10^{-6}$ for merging BIC at (b) Γ point and (c) off-Γ point. Other structural parameters are the same as in Fig. 2 and Fig. 3 for $a = 1101$ nm and $a = 1083$ nm, respectively.

Funding. National Key Research and Development Program of China (2021YFA1400602); National Natural Science Foundation of China (11974261, 12104105, 12274325, 61621001, 62075213, 91850206); Fundamental Research Funds for the Central Universities (22120190222).

Disclosures. The authors declare no conflicts of interest.

Data Availability. Data underlying the results presented in this paper are not publicly available at this time but may be obtained from the authors upon reasonable request.

REFERENCES

1. A. E. Miroshnichenko, A. B. Evlyukhin, Y. F. Yu, R. M. Bakker, A. Chipouline, A. I. Kuznetsov, B. Luk'yanchuk, B. N. Chichkov, and Y. S. Kivshar, "Nonradiating anapole modes in dielectric nanoparticles," Nat. Commun. **6**, 8069 (2015).
2. B. S. Song, S. Noda, T. Asano, and Y. Akahane, "Ultra-high-Q photonic double-heterostructure nanocavity," Nat. Mater. **4**, 207–210 (2005).
3. J. Tian, Q. Li, P. A. Belov, R. K. Sinha, W. Qian, and M. Qiu, "High-Q all-dielectric metasurface: super and suppressed optical absorption," ACS Photon. **7**, 1436–1443 (2020).
4. S. Jahani and Z. Jacob, "All-dielectric metamaterials," Nat. Nanotechnol. **11**, 23–36 (2016).
5. M. F. Limonov, M. V. Rybin, A. N. Poddubny, and Y. S. Kivshar, "Fano resonances in photonics," Nat. Photonics **11**, 543–554 (2017).
6. I. Staude and J. Schilling, "Metamaterial-inspired silicon nanophotonics," Nat. Photonics **11**, 274–284 (2017).
7. W. Zhou, D. Zhao, Y. C. Shuai, H. Yang, S. Chuwongin, A. Chadha, J. H. Seo, K. X. Wang, V. Liu, Z. Ma, and S. Fan, "Progress in 2D photonic crystal Fano resonance photonics," Prog. Quantum Electron. **38**, 1–74 (2014).
8. C. W. Hsu, B. Zhen, A. D. Stone, J. D. Joannopoulos, and M. Soljačić, "Bound states in the continuum," Nat. Rev. Mater. **1**, 16408 (2016).
9. A. F. Sadreev, "Interference traps waves in an open system: bound states in the continuum," Rep. Prog. Phys. **84**, 055901 (2021).
10. K. Koshelev, G. Favraud, A. Bogdanov, Y. Kivshar, and A. Fratalocchi, "Nonradiating photonics with resonant dielectric nanostructures," Nanophotonics **8**, 725–745 (2019).
11. H. Friedrich and D. Wintgen, "Interfering resonances and bound states in the continuum," Phys. Rev. A **32**, 3231–3242 (1985).
12. M. I. Molina, A. E. Miroshnichenko, and Y. S. Kivshar, "Surface bound states in the continuum," Phys. Rev. Lett. **108**, 070401 (2012).
13. G. Corrielli, G. Della Valle, A. Crespi, R. Osellame, and S. Longhi, "Observation of surface states with algebraic localization," Phys. Rev. Lett. **111**, 220403 (2013).
14. R. Porter and D. V. Evans, "Water-wave trapping by floating circular cylinders," J. Fluid Mech. **633**, 311–325 (2009).
15. P. J. Cobelli, V. Pagneux, A. Maurel, and P. Petitjeans, "Experimental study on water-wave trapped modes," J. Fluid Mech. **666**, 445–476 (2011).
16. F. Wu, J. Wu, Z. Guo, H. Jiang, Y. Sun, Y. Li, J. Ren, and H. Chen, "Giant enhancement of the Goos-Hänchen shift assisted by quasi-bound states in the continuum," Phys. Rev. Appl. **12**, 014028 (2019).
17. F. Wu, M. Luo, J. Wu, C. Fan, X. Qi, Y. Jian, D. Liu, S. Xiao, G. Chen, H. Jiang, Y. Sun, and H. Chen, "Dual quasibound states in the continuum in compound grating waveguide structures for large positive and negative Goos-Hänchen shifts with perfect reflection," Phys. Rev. A **104**, 023518 (2021).
18. J. Wu, X. Xu, X. Su, S. Zhao, C. Wu, Y. Sun, Y. Li, F. Wu, Z. Guo, H. Jiang, and H. Chen, "Observation of giant extrinsic chirality empowered by quasi-bound states in the continuum," Phys. Rev. Appl. **16**, 064018 (2021).
19. Z. Li, Y. Xiang, S. Xu, and X. Dai, "Ultrasensitive terahertz sensing in all-dielectric asymmetric metasurfaces based on quasi-BIC," J. Opt. Soc. Am. B **39**, 286–291 (2022).
20. A. Overvig, N. Yu, and A. Alù, "Chiral quasi-bound states in the continuum," Phys. Rev. Lett. **126**, 073001 (2021).
21. Z. Zhang, F. Qin, Y. Xu, S. Fu, Y. Wang, and Y. Qin, "Negative refraction mediated by bound states in the continuum," Photon. Res. **9**, 1592–1597 (2021).
22. L. Huang, B. Jia, Y. K. Chiang, S. Huang, C. Shen, F. Deng, T. Yang, D. A. Powell, Y. Li, and A. E. Miroshnichenko, "Topological supercavity resonances in the finite system," Sci. Adv. **9**, 2200257 (2022).
23. A. A. Lyapina, D. N. Maksimov, A. S. Pilipchuk, and A. F. Sadreev, "Bound states in the continuum in open acoustic resonators," J. Fluid Mech. **780**, 370–387 (2015).
24. L. Huang, Y. K. Chiang, S. Huang, C. Shen, F. Deng, Y. Cheng, B. Jia, Y. Li, D. A. Powell, and A. E. Miroshnichenko, "Sound trapping in an open resonator," Nat. Commun. **12**, 4819 (2021).
25. I. Deriy, I. Toftul, M. Petrov, and A. Bogdanov, "Bound states in the continuum in compact acoustic resonators," Phys. Rev. Lett. **128**, 084301 (2022).
26. Z. G. Chen, C. Xu, R. Al Jahdali, J. Mei, and Y. Wu, "Corner states in a second-order acoustic topological insulator as bound states in the continuum," Phys. Rev. B **100**, 075120 (2019).
27. E. N. Bulgakov and A. F. Sadreev, "Bound states in the continuum in photonic waveguides inspired by defects," Phys. Rev. B **78**, 075105 (2008).
28. K. Koshelev, S. Lepeshov, M. Liu, A. Bogdanov, and Y. Kivshar, "Asymmetric metasurfaces with high-Q resonances governed by bound states in the continuum," Phys. Rev. Lett. **121**, 193903 (2018).
29. Z. Liu, Y. Xu, Y. Lin, J. Xiang, T. Feng, Q. Cao, J. Li, S. Lan, and J. Liu, "High-Q quasibound states in the continuum for nonlinear metasurfaces," Phys. Rev. Lett. **123**, 253901 (2019).
30. K. Koshelev, Y. Tang, K. Li, D. Y. Choi, G. Li, and Y. Kivshar, "Nonlinear metasurfaces governed by bound states in the continuum," ACS Photon. **6**, 1639–1644 (2019).
31. Y. Lin, T. Feng, S. Lan, J. Liu, and Y. Xu, "On-chip diffraction-free beam guiding beyond the light cone," Phys. Rev. Appl. **13**, 064032 (2020).

32. Y. Xie, Z. Zhang, Y. Lin, T. Feng, and Y. Xu, "Magnetic quasi-bound state in the continuum for wireless power transfer," Phys. Rev. Appl. **15**, 044024 (2021).
33. X. Yin, J. Jin, M. Soljačić, C. Peng, and B. Zhen, "Observation of topologically enabled unidirectional guided resonances," Nature **580**, 467–471 (2020).
34. M. S. Hwang, H. C. Lee, K. H. Kim, K. Y. Jeong, S. H. Kwon, K. Koshelev, Y. Kivshar, and H. G. Park, "Ultralow-threshold laser using super-bound states in the continuum," Nat. Commun. **12**, 4135 (2021).
35. J. H. Yang, Z. T. Huang, D. N. Maksimov, P. S. Pankin, I. V. Timofeev, K. B. Hong, H. Li, J. W. Chen, C. Y. Hsu, Y. Y. Liu, T. C. Lu, T. R. Lin, C. S. Yang, and K. P. Chen, "Low-threshold bound state in the continuum lasers in hybrid lattice resonance metasurfaces," Laser Photon. Rev. **15**, 2100118 (2021).
36. Z. Wang, Q. Xue, S. Zhao, X. Zhang, H. Liu, and X. Sun, "Study on the characteristics of a photonic crystal sensor with rectangular lattice based on bound states in the continuum," J. Phys. D **55**, 175106 (2022).
37. P. Hu, C. Xie, Q. Song, A. Chen, H. Xiang, D. Han, and J. Zi, "Bound states in the continuum based on the total internal reflection of Bloch waves," Natl. Sci. Rev. **10**, nwac043 (2023).
38. S. Dai, L. Liu, D. Han, and J. Zi, "From topologically protected coherent perfect reflection to bound states in the continuum," Phys. Rev. B **98**, 081405 (2018).
39. B. Wang, W. Liu, M. Zhao, J. Wang, Y. Zhang, A. Chen, F. Guan, X. Liu, L. Shi, and J. Zi, "Generating optical vortex beams by momentum-space polarization vortices centered at bound states in the continuum," Nat. Photonics **14**, 623–628 (2020).
40. W. Liu, B. Wang, Y. Zhang, J. Wang, M. Zhao, F. Guan, X. Liu, L. Shi, and J. Zi, "Circularly polarized states spawning from bound states in the continuum," Phys. Rev. Lett. **123**, 116104 (2019).
41. J. Wang, L. Shi, and J. Zi, "Spin hall effect of light via momentum-space topological vortices around bound states in the continuum," Phys. Rev. Lett. **129**, 236101 (2022).
42. H. Barkaoui, K. Du, Y. Chen, S. Xiao, and Q. Song, "Merged bound states in the continuum for giant superchiral field and chiral mode splitting," Phys. Rev. B **107**, 045305 (2023).
43. Y. Chen, H. Deng, X. Sha, W. Chen, R. Wang, Y. H. Chen, D. Wu, J. Chu, Y. S. Kivshar, S. Xiao, and C. W. Qiu, "Observation of intrinsic chiral bound states in the continuum," Nature **613**, 474–478 (2023).
44. M. Minkov, I. A. D. Williamson, M. Xiao, and S. Fan, "Zero-index bound states in the continuum," Phys. Rev. Lett. **121**, 263901 (2018).
45. Z. Sadrieva, K. Frizyuk, M. Petrov, Y. Kivshar, and A. Bogdanov, "Multipolar origin of bound states in the continuum," Phys. Rev. B **100**, 115303 (2019).
46. M. S. Sidorenko, O. N. Sergaeva, Z. F. Sadrieva, C. Roques-Carmes, P. S. Muraev, D. N. Maksimov, and A. A. Bogdanov, "Observation of an accidental bound state in the continuum in a chain of dielectric disks," Phys. Rev. Appl. **15**, 034041 (2021).
47. D. R. Abujetas, J. Olmos-Trigo, and J. A. Sánchez-Gil, "Tailoring accidental double bound states in the continuum in all-dielectric metasurfaces," Adv. Opt. Mater. **10**, 2200301 (2022).
48. P. Hu, J. Wang, Q. Jiang, J. Wang, L. Shi, D. Han, Z. Q. Zhang, C. T. Chan, and J. Zi, "Global phase diagram of bound states in the continuum," Optica **9**, 1353–1361 (2022).
49. W. Ye, Y. Gao, and J. Liu, "Singular points of polarizations in the momentum space of photonic crystal slabs," Phys. Rev. Lett. **124**, 153904 (2020).
50. B. Zhen, C. W. Hsu, L. Lu, A. D. Stone, and M. Soljačić, "Topological nature of optical bound states in the continuum," Phys. Rev. Lett. **113**, 257401 (2014).
51. A. Chen, W. Liu, Y. Zhang, B. Wang, X. Liu, L. Shi, L. Lu, and J. Zi, "Observing vortex polarization singularities at optical band degeneracies," Phys. Rev. B **99**, 180101 (2019).
52. T. Yoda and M. Notomi, "Generation and annihilation of topologically protected bound states in the continuum and circularly polarized states by symmetry breaking," Phys. Rev. Lett. **125**, 053902 (2020).
53. J. Jin, X. Yin, L. Ni, M. Soljačić, B. Zhen, and C. Peng, "Topologically enabled ultrahigh-*Q* guided resonances robust to out-of-plane scattering," Nature **574**, 501–504 (2019).
54. M. Kang, L. Mao, S. Zhang, M. Xiao, H. Xu, and C. T. Chan, "Merging bound states in the continuum by harnessing higher-order topological charges," Light Sci. Appl. **11**, 228 (2022).
55. M. Kang, S. Zhang, M. Xiao, and H. Xu, "Merging bound states in the continuum at off-high symmetry points," Phys. Rev. Lett. **126**, 117402 (2021).
56. L. Huang, W. Zhang, and X. Zhang, "Moiré quasibound states in the continuum," Phys. Rev. Lett. **128**, 253901 (2022).
57. Q. Song, J. Hu, S. Dai, C. Zheng, D. Han, J. Zi, Z. Q. Zhang, and C. T. Chan, "Coexistence of a new type of bound state in the continuum and a lasing threshold mode induced by PT symmetry," Sci. Adv. **6**, 1160 (2020).
58. Y. Yu, A. Sakanas, A. R. Zali, E. Semenova, K. Yvind, and J. Mørk, "Ultra-coherent Fano laser based on a bound state in the continuum," Nat. Photonics **15**, 758–764 (2021).
59. F. Yesilkoy, E. R. Arvelo, Y. Jahani, M. Liu, A. Tittl, V. Cevher, Y. Kivshar, and H. Altug, "Ultrasensitive hyperspectral imaging and biodetection enabled by dielectric metasurfaces," Nat. Photonics **13**, 390–396 (2019).
60. Y. Wang, Z. Han, Y. Du, and J. Qin, "Ultrasensitive terahertz sensing with high-*Q* toroidal dipole resonance governed by bound states in the continuum in all-dielectric metasurface," Nanophotonics **10**, 1295–1307 (2021).
61. V. Kravtsov, E. Khestanova, F. A. Benimetskiy, T. Ivanova, A. K. Samusev, I. S. Sinev, D. Pidgayko, A. M. Mozharov, I. S. Mukhin, M. S. Lozhkin, Y. V. Kapitonov, A. S. Brichkin, V. D. Kulakovskii, I. A. Shelykh, A. I. Tartakovskii, P. M. Walker, M. S. Skolnick, D. N. Krizhanovskii, and I. V. Iorsh, "Nonlinear polaritons in a monolayer semiconductor coupled to optical bound states in the continuum," Light Sci. Appl. **9**, 56 (2020).
62. M. Minkov, D. Gerace, and S. Fan, "Doubly resonant $\chi^{(2)}$ nonlinear photonic crystal cavity based on a bound state in the continuum," Optica **6**, 1039–1045 (2019).
63. K. Koshelev, S. Kruk, E. M. Gaykazyan, J. H. Choi, A. Bogdanov, H. G. Park, and Y. Kivshar, "Subwavelength dielectric resonators for nonlinear nanophotonics," Science **367**, 288–292 (2020).
64. L. L. Doskolovich, E. A. Bezus, and D. A. Bykov, "Integrated flat-top reflection filters operating near bound states in the continuum," Photon. Res. **7**, 1314–1322 (2019).
65. C. Zhao, W. Chen, J. Wei, W. Deng, Y. Yan, Y. Zhang, and C. W. Qiu, "Electrically tunable and robust bound states in the continuum enabled by 2D transition metal dichalcogenide," Adv. Opt. Mater. **10**, 2201634 (2022).
66. T. Kaelberer, V. Fedotov, N. Papasimakis, D. Tsai, and N. Zheludev, "Toroidal dipolar response in a metamaterial," Science **330**, 1510–1512 (2010).
67. S. Han, L. Cong, Y. K. Srivastava, B. Qiang, M. V. Rybin, A. Kumar, R. Jain, W. X. Lim, V. G. Achanta, S. S. Prabhu, Q. J. Wang, Y. S. Kivshar, and R. Singh, "All-dielectric active terahertz photonics driven by bound states in the continuum," Adv. Mater. **31**, 1901921 (2019).
68. M. V. Rybin, D. S. Filonov, K. B. Samusev, P. A. Belov, Y. S. Kivshar, and M. F. Limonov, "Phase diagram for the transition from photonic crystals to dielectric metamaterials," Nat. Commun. **6**, 10102 (2015).
69. S. Gehrsitz, F. K. Reinhart, C. Gourgon, N. Herres, A. Vonlanthen, and H. Sigg, "The refractive index of $Al_xGa_{1-x}As$ below the band gap: accurate determination and empirical modeling," J. Appl. Phys. **87**, 7825 (2000).
70. Z. Yang, P. Chak, A. D. Bristow, H. Driel, and J. E. Sipe, "Enhanced second-harmonic generation in AlGaAs microring resonators," Opt. Lett. **32**, 826–828 (2007).
71. N. Bernhardt, K. Koshelev, S. J. U. White, K. W. C. Meng, J. E. Froch, S. Kim, T. T. Tran, D. Y. Choi, Y. Kivshar, and A. S. Solntsev, "Quasi-BIC resonant enhancement of second-harmonic generation in WS_2 monolayers," Nano Lett. **20**, 5309–5314 (2020).
72. C. Fang, Q. Yang, Q. Yuan, L. Gu, X. Gan, Y. Shao, Y. Liu, G. Han, and Y. Hao, "Efficient second-harmonic generation from silicon slotted nanocubes with bound states in the continuum," Laser Photon. Rev. **16**, 2100498 (2022).
73. L. Kang, H. Bao, and D. H. Werner, "Efficient second-harmonic generation in high *Q*-factor asymmetric lithium niobate metasurfaces," Opt. Lett. **46**, 633–636 (2021).